Alzheimer's & Dementia: Translational Research & Clinical Interventions 3 (2017) 542-552

Featured Article

Biomathematical screening of amyloid radiotracers with clinical usefulness index

Ying-Hwey Nai[a,b], Miho Shidahara[c], Chie Seki[d], Hiroshi Watabe[a,b,*]

[a]*Division of Radiation Informatics for Medical Imaging, Graduate School of Biomedical Engineering, Tohoku University, Sendai, Japan*
[b]*Division of Radiation Protection and Safety Control, Cyclotron and Radioisotope Center, Tohoku University, Sendai, Japan*
[c]*Department of Medical Physics, Graduate School of Medicine, Tohoku University, Sendai, Japan*
[d]*Department of Functional Brain Imaging Research, National Institute of Radiological Sciences, National Institutes for Quantum and Radiological Science and Technology, Chiba, Japan*

Abstract

Introduction: To facilitate radiotracers' development, a screening methodology using a biomathematical model and clinical usefulness index (CUI) was proposed to evaluate radiotracers' diagnostic capabilities.

Methods: A total of 31 amyloid positron emission tomography radiotracers were evaluated. A previously developed biomathematical model was used to simulate 1000 standardized uptake value ratios with population and noise simulations, which were used to determine the integrated receiver operating characteristics curve (Az), effect size (Es), and standardized uptake value ratio (Sr) of conditions-pairs of healthy control–mild cognitive impaired and mild cognitive impaired–Alzheimer's disease. CUI was obtained from the product of averaged Az($\overline{\text{Az}}$), Es($\overline{\text{Es}}$), and Sr($\overline{\text{Sr}}$).

Results: The relationships of $\overline{\text{Az}}$, $\overline{\text{Es}}$, and $\overline{\text{Sr}}$ with CUI were different, suggesting that they assessed different radiotracer properties. The combination of Az, Es, and Sr complemented each other and resulted in CUI of 0.10 to 5.72, with clinically applied amyloid positron emission tomography radiotracers having CUI greater than 3.0.

Discussion: The CUI rankings of clinically applied radiotracers were close to their reported clinical results, attesting to the applicability of the screening methodology.

Keywords: Alzheimer's disease; Amyloid; Biomathematical model; Clinical usefulness; Positron emission tomography (PET)

1. Introduction

Amyloid imaging, using positron emission tomography (PET), provides in vivo imaging of the cerebral amyloid load in an individual. As amyloid load shows greater changes in the early stages of Alzheimer's disease (AD) [1], amyloid imaging allows for early diagnosis of possible AD conversion and differential diagnosis of various neurodegenerative diseases. To quantify the amyloid load, standardized uptake value ratio (SUVR) is commonly used with thresholds established to classify the subjects into amyloid β (Aβ) positive or negative [2–5]. An individual classified as Aβ-positive has high SUVR in cortical areas. This indicates a high amount of amyloid fibrils, and hence a high probability of cognitive

Software: A software written in Matlab for screening radiotracers using the proposed screening methodology and clinical usefulness index is available: http://www.rim.cyric.tohoku.ac.jp/software/CUI-Software.

Ethical approval: This article does not contain any studies with human participants or animals performed by any of the authors.

Conflict of interest: The authors declare that they have no conflicts of interest.

*Corresponding author. Tel.: +81-22-795-7803; Fax: +81-22-795-7809.

E-mail address: hwatabe@m.tohoku.ac.jp

http://dx.doi.org/10.1016/j.trci.2017.08.006

impairment. In contrast, an individual classified as Aβ-negative has sparse to nondetectable amount of amyloid fibrils and a low possibility of cognitive impairment [2]. The greater the SUVR differences between two conditions, the easier it is to set thresholds for diagnosing the subjects with higher accuracy. However, this is dependent on the radiotracers whereby good radiotracers show clear differences between the subject conditions and vice versa for poorer tracers.

The development of a successful diagnostic radiotracer is hampered by the limitations of conventional radiotracers' development process [6]. It is a long, tedious, and iterative process of identifying the right chemical compounds, followed by lead optimization via iterative processes of conducting multiple in vitro experiments and preclinical testing before clinical testing [6]. Moreover, it focuses on a few physicochemical or pharmacologic properties (e.g., lipophilicity, selectivity to target sites) to evaluate radiotracers [6,7]. In vitro and preclinical results may not translate well to clinical performance because of the lack of consideration to the possible in vivo kinetics of the radiotracers during development [6,7].

Previously, we had developed a biomathematical model to predict the in vivo binding capability of amyloid PET radiotracers in terms of cortical SUVR, under healthy control (HC) and AD conditions, representing Aβ-negative and Aβ-positive diagnosis [8]. In this study, we proposed a screening methodology using amyloid PET radiotracers by extending the previous model to include the noise level of the imaging modality, population variation, and clinical usefulness evaluation [8]. As SUVR was used to measure amyloid load in clinical studies, it was chosen as the outcome parameter of interest [8].

Clinical usefulness reflects the diagnostic capability of a radiotracer to differentiate the subject conditions. Conventionally, it is evaluated using methods such as receiver operating characteristics (ROCs) and effect size. ROC evaluates the sensitivity and specificity of a radiotracer in diagnosing the subjects' conditions correctly [9]. Effect size is used to determine the strength of the differences in measured values between two subject groups [10]. In amyloid imaging, differences in SUVRs between HC and AD are often used [2,4].

To support decision-making in moving candidate radiotracers for clinical evaluation, the use of a common index can help in comparing candidate radiotracers from within and across institutions, and with clinically applied radiotracers. In this study, a clinical usefulness index (CUI) was proposed for objective evaluation of the diagnostic power of the radiotracer in differentiating subjects, based on its cortical binding capability, in terms of SUVR. The range of amyloid loads between representative subject conditions of HC and mild cognitive impaired (MCI) and between MCI and AD was used to represent the conditions of low and high amyloid loads, respectively. CUI was defined as the product of the averaged of the area under the ROC curve (Az), effect size (Es), and SUVR ratios (Sr) of conditions-pairs of HC-MCI and MCI-AD. The relationships among Az, Es, Sr, and CUI were investigated. The feasibility of the screening methodology with CUI was investigated by comparing the ranking of CUI values with clinical results of clinically applied amyloid PET radiotracers.

2. Materials and methods

The proposed screening methodology (Fig. 1) consisted of the previously developed amyloid biomathematical model [8] (Fig. 1A), with population and noise simulations, and tracer evaluation based on CUI (Fig. 1B). A total of 31 (12 clinically applied and 19 candidates) amyloid PET radiotracers were evaluated (Table 1).

2.1. Amyloid biomathematical model

Details of the biomathematical model used in this study are found elsewhere [8]. We briefly summarize the model in predicting SUVR in the following sections.

2.1.1. Generation of physicochemical and pharmacologic parameters

Molecular volume and lipophilicity of each radiotracer were represented by McGowan volume (V_x, cm^3/mol/100) and Moriguchi log P (M log P, unitless), which were generated based on the chemical structure of the radiotracer using commercial software, dproperties (Talete, Italy). In silico free fractions of the radiotracer in tissues (f_{ND}, unitless) and in plasma (f_p, unitless) were calculated using M log P, from the following relationships [8]:

$$f_{ND} = 7.717e^{-1.634 \cdot \mathrm{MlogP}} \quad (1)$$

$$f_p = 0.936 \cdot {f_{ND}}^{0.600} \quad (2)$$

Dissociation constant, K_D, the only in vitro parameter, was extracted from the literature (Table 1). Fixed available target binding sites (B_{avail}) of 4, 20, and 50 nM were used to represent the amyloid loads under HC, MCI, and AD conditions, respectively [40].

2.1.2. Derivation of 1-tissue-compartment model kinetic parameters

The biomathematical model (Fig. 1A) was based on a simplified 1-tissue-compartment model, assuming that the radiotracers cross the blood-brain barrier by passive diffusion [7,8]. The influx rate constant (K_1, mL/cm^3/minutes) was derived using the modified Renkin and Crone equation, with compound-specific permeability (P, cm/minutes) and fixed values of capillary surface area (S = 150 cm^2/cm^3 of brain) and perfusion (f = 0.6 mL/cm^3/minutes) as follows [7]:

$$K_1 = f\left(1 - e^{\frac{-PS}{f}}\right) \quad (3)$$

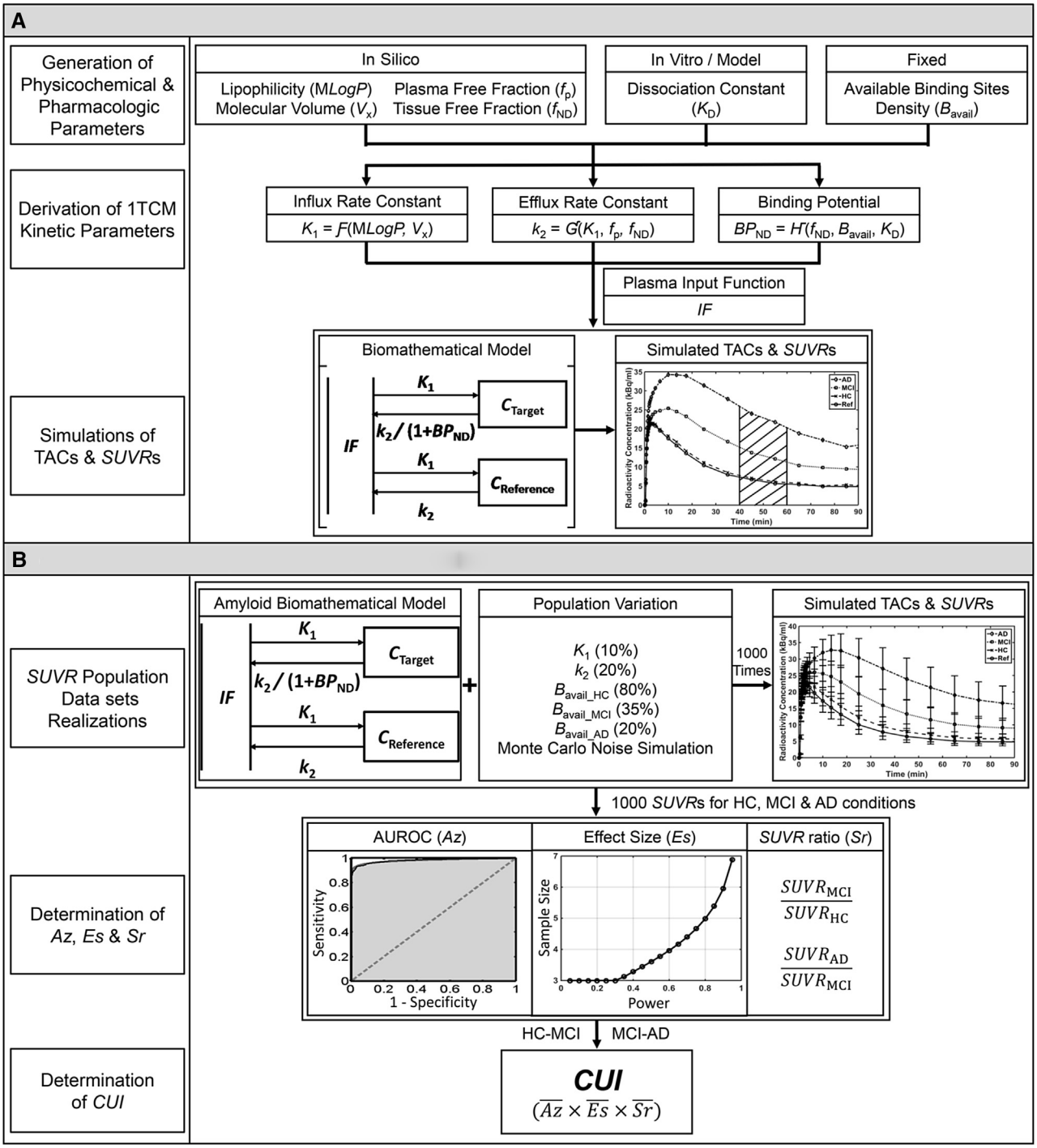

Fig. 1. Overview of the proposed screening methodology for amyloid positron emission tomography radiotracers. (A) Amyloid biomathematical model; (B) amyloid radiotracers' screening methodology. Abbreviations: AD, Alzheimer's disease; AUROC, area under the receiver operating characteristic curve; CUI, clinical usefulness index; HC, healthy control; IF, input function; MCI, mild cognitive impaired; SUVR, standardized uptake value ratio; TACs, time activity curves; 1TCM, 1-tissue-compartment model.

The compound-specific permeability was derived from the simplified Lanevskij's permeability model [7], using M log P and V_x [8]:

$$P = 10^{-0.121(\mathrm{M}\log P - 2.298)^2 - 2.544 \log\left(V_x^{1/3}\right) - 2.525} \quad (4)$$

At equilibrium, the efflux rate constant (k_2, minutes^{-1}) can be derived using K_1, f_p, and f_{ND} [7]:

$$k_2 = \frac{f_{ND}}{f_p} \cdot K_1 \quad (5)$$

Table 1
In silico M log *P*, V_x, f_p, and f_{ND}, and in vitro K_D of 31 amyloid PET radiotracers

	In silico				In vitro K_D				
Radiotracers	M log *P*	V_x	f_p	f_{ND}	Synthetic $A\beta_{1-40}$	Synthetic $A\beta_{1-42}$	AD brain homogenates	K_D for simulations	References
[^{11}C]PIB	*2.40*	*1.88*	*0.303*	*0.152*	2.48*	0.930*		*1.40*†	[11–14]
[^{18}F]FDDNP	*2.89*	*2.31*	*0.187*	*0.068*	0.120	5.52		*3.90*†	[15,16]
[^{11}C]SB13	*3.23*	*1.86*	*0.135*	*0.040*			2.43	*2.43*	[17]
[^{18}F]florbetaben	*3.11*	*2.84*	*0.152*	*0.048*			2.22‡	*2.22*	[18]
[^{11}C]BF227	*2.40*	*2.33*	*0.304*	*0.153*	1.80§	4.30§		*3.55*†	[19]
[^{18}F]AV138	*3.11*	*2.80*	*0.152*	*0.048*			1.90¶	*1.90*	[20]
[^{18}F]flutemetamol	*2.80*	*1.89*	*0.205*	*0.080*	1.60			*1.60*	[21]
[^{18}F]florbetapir	*2.52*	*2.80*	*0.270*	*0.126*			3.72	*3.72*	[18]
[^{11}C]AZD2184	*1.75*	*1.84*	*0.573*	*0.441*	8.40			*8.40*	[14]
[^{18}F]flutafuranol	*2.41*	*1.79*	*0.300*	*0.150*	2.30			*2.30*	[21]
[^{18}F]FACT	*1.87*	*2.53*	*0.511*	*0.365*	9.40			*9.40*	[22]
[^{18}F]FIBT	*3.04*	*2.41*	*0.162*	*0.054*			0.700	*0.700*	[23]
[^{11}C]6-Me-BTA-1	*3.23*	*1.96*	*0.135*	*0.040*	20.2¶			*20.2*	[24]
[^{11}C]BTA-1	*2.97*	*1.82*	*0.173*	*0.060*	11.0¶			*11.0*	[25]
[^{18}F]FMAPO	*3.47*	*2.50*	*0.107*	*0.027*			5.00¶	*5.00*	[26]
[^{18}F]FPEG-stilbenes-12a#	*3.47*	*2.50*	*0.107*	*0.027*			2.90¶	*2.90*	[27]
[^{11}C]Benzofuran-8#	*2.66*	*1.81*	*0.236*	*0.100*			0.700¶	*0.700*	[28]
[^{18}F]FPEGN3-styrylpyridine-2#	*3.74*	*2.94*	*0.082*	*0.017*			2.50¶	*2.50*	[29]
[^{11}C]MeS-IMPY	*3.33*	*2.20*	*0.122*	*0.034*			8.95¶	*8.95*	[30]
[^{18}F]Indole-14#	*2.98*	*2.79*	*0.172*	*0.060*			1.50¶	*1.50*	[31]
[^{18}F]Indoline-8#	*2.93*	*2.83*	*0.180*	*0.064*			4.00¶	*4.00*	[31]
[^{11}C]Benzothiazole-6a#	*2.40*	*1.88*	*0.303*	*0.152*			18.8¶	*18.8*	[32]
[^{11}C]Benzothiazole-6b#	*2.40*	*1.88*	*0.303*	*0.152*			11.5¶	*11.5*	[32]
[^{11}C]Benzothiazole-6c#	*2.40*	*1.88*	*0.303*	*0.152*			11.2¶	*11.2*	[32]
[^{18}F]Benzothiazole-2#	*3.72*	*1.59*	*0.083*	*0.018*			9.00¶	*9.00*	[33]
[^{18}F]Benzothiazole-5#	*3.98*	*1.74*	*0.064*	*0.012*			5.70¶	*5.70*	[34]
[^{18}F]MK3328	*2.63*	*1.78*	*0.241*	*0.104*			9.60	*9.60*	[35]
[^{18}F]FIAR	*3.66*	*2.29*	*0.088*	*0.020*		6.81¶		*6.81*	[36]
[^{18}F]Benzoxazole-24#	*2.41*	*2.75*	*0.302*	*0.152*		9.30¶		*9.30*	[37]
[^{18}F]Pyridinylbenzoxazole-32#	*2.42*	*2.03*	*0.297*	*0.148*		8.00¶		*8.00*	[38]
[^{18}F]Phenylindole-1a#	*3.84*	*2.09*	*0.074*	*0.015*		28.4¶		*28.4*	[39]

Abbreviations: AD, Alzheimer's disease; Aβ, amyloid beta; PET, positron emission tomography.

NOTE. The final values used for simulations are italicized. The amyloid PET radiotracers listed from [^{11}C]PIB to [^{18}F]FIBT are applied clinically, whereas the rest are candidate radiotracers. M log *P* (unitless) and V_x (cm^3/mol/100) were determined using dproperties (Talete, Italy). f_p (unitless) and f_{ND} (unitless) were extrapolated from relationships of f_p and f_{ND} of CNS tracers. K_D (nM) was obtained from the literature, measured via in vitro binding studies with synthetic $A\beta_{1-40}$, $A\beta_{1-42}$, or AD brain homogenates.

*$K_{D(A\beta1-40)}$ was averaged from four literature values (1.02 [12], 0.90 [13], 3.30 [14], and 4.70 [11]) and $K_{D(A\beta1-42)}$ was averaged from two literature values (0.91 [12] and 0.95 [13]).

†K_D is derived using K_D measured with synthetic $A\beta_{1-40}$ and $A\beta_{1-42}$ using: $K_{D(A\beta1-40)} \times 0.3 + K_{D(A\beta1-42)} \times 0.7$.

‡K_i measured with florbetapir as the competitor.

§K_i measured with BF180 as the competitor; BF180 exhibits similar binding to IMPY [19].

¶K_i measured with itself or IMPY as the competitor.

#Simplified name with a number or alphabet, as reported in the literature, used when generic name or institute code name was not available.

The in vivo nondisplaceable binding potential (BP_{ND}, unitless) was derived from Mintun's equation using B_{avail}, f_{ND}, and K_D [7]:

$$BP_{ND} = f_{ND} \cdot \frac{B_{avail}}{K_D} \quad (6)$$

Three scaling factors of 1.23, 1.15, and 0.38 were introduced to account for the difference between in silico and in vivo K_1, k_2, and BP_{ND} in equations (3), (5), and (6), respectively. These scaling factors were derived by minimizing the differences between the predicted and clinically observed K_1, k_2, and BP_{ND} of 8, 8, and 9 clinically applied radiotracers in AD [8] (Fig. 2).

2.1.3. Simulations of time activity curves and SUVRs

The predicted K_1, k_2, and BP_{ND} were used to simulate the time activity curves (TACs) in the target regions of HC, MCI, and AD and a reference region, with a fixed arterial input function (IF) [8]:

$$C_{Target}(t) = K_1 \cdot e^{(-k_2/(1+BP_{ND}))t} \otimes IF(t) \quad (7)$$

$$C_{\text{Reference}}(t) = K_1 \cdot e^{-k_2 t} \otimes \text{IF}(t) \quad (8)$$

IF was derived by averaging the metabolite-corrected, arterial plasma IFs of six HC subjects injected with [^{11}C]BF227 [8,41].

SUVRs of subject conditions of HC, MCI, and AD were determined from the ratio of integrated TACs of the target regions in HC, MCI, and AD and that of the reference region within the selected time window. The time window was determined from the literature for clinically applied amyloid PET radiotracers [8], 70 to 90 minutes for [^{18}F]FIBT [42] or otherwise by default of 40 to 60 minutes. The same IF was applied assuming a reference region without any specific binding in our simulations, hence eliminating any complications in evaluating the binding capability of the radiotracer due to changes in subject physiology.

2.2. Amyloid PET radiotracers' screening methodology

2.2.1. SUVR population data set realizations

To simulate clinical situations, K_1 and k_2 predicted from equations (3) and (5) were varied by 10% and 20%, respectively [43]. B_{avail} was varied by 80%, 35%, and 20% under HC, MCI, and AD conditions, respectively [40]. One thousand noisy TACs in both target and reference regions were generated by computer simulations. The noise was simulated such that the averaged noise level from 8 to 150 minutes was 3% [44,45], which reflects the noise level of typical PET data. The 1000 TACs simulated for both target and reference regions were used to obtain 1000 SUVRs for each subject condition of HC, MCI, and AD. Simulations were carried out using in-house software written in Matlab (Ver. R2014b, The MathWorks Inc, USA).

2.2.2. Determination of Az, Es, and Sr

Az, Es, and Sr were determined for each conditions-pair of HC-MCI and MCI-AD using the 1000 SUVRs of subject conditions of HC, MCI, and AD. Az was derived using an ROC program written in Matlab. For each conditions-pair, thresholds were generated for the differences between all SUVR values. Az was then determined from the area under the ROC curve generated using the sensitivity and specificity determined for each threshold. Es was determined using the means (M) and standard deviations (SDs) of 1000 SUVRs of subject conditions of HC, MCI, and AD in pairs of HC-MCI and MCI-AD:

$$\text{Es}_{1-2} = \frac{(M_2 - M_1)}{\sqrt{(\text{SD}_2^2 + \text{SD}_1^2)/2}} \quad (9)$$

where 1 = HC and 2 = MCI for conditions-pair of HC-MCI, and 1 = MCI and 2 = AD for conditions-pair of MCI-AD. Sr was determined by dividing M of 1000 SUVRs for subject conditions of HC, MCI, and AD accordingly to obtain $\text{Sr}_{\text{MCI/HC}}$ and $\text{Sr}_{\text{AD/MCI}}$ for conditions-pairs of HC-MCI and MCI-AD.

2.2.3. Determination of CUI

CUI was obtained from the product of the averaged Az($\overline{\text{Az}}$), Es($\overline{\text{Es}}$), and Sr($\overline{\text{Sr}}$) of conditions-pairs of HC-MCI and MCI-AD as follows:

$$\text{CUI} = \frac{1}{2}(\text{Az}_{\text{HC-MCI}} + \text{Az}_{\text{MCI-AD}}) \times \frac{1}{2}(\text{Es}_{\text{HC-MCI}} + \text{Es}_{\text{MCI-AD}}) \times \frac{1}{2}(\text{Sr}_{\text{MCI/HC}} + \text{Sr}_{\text{AD/MCI}}) = \overline{\text{Az}} \times \overline{\text{Es}} \times \overline{\text{Sr}} \quad (10)$$

Equal weightage was applied, indicating that the binding capabilities to low and high amyloid loads were equally important in evaluating the performance of the amyloid PET radiotracer.

2.3. Comparison of amyloid PET radiotracers based on CUI

The CUIs of 31 amyloid PET radiotracers (Table 1) were ranked from highest to lowest. The relationships among $\overline{\text{Az}}$, $\overline{\text{Es}}$, $\overline{\text{Sr}}$, and the resulting CUI for the listed radiotracers were investigated.

3. Results

CUI ranged from 0.10 to 5.72 for the 31 amyloid PET radiotracers evaluated (Table 2). Az ranged from 0.55 to 0.99, Es ranged from 0.17 to 3.64, and Sr ranged from 1.00 to 1.89, for conditions-pairs of HC-MCI and MCI-AD (Table 2). Smaller Az, Es, and Sr were generally observed for conditions-pair of HC-MCI compared with that of MCI-AD (Table 2). Among the clinically applied amyloid PET radiotracers, [^{11}C]PIB was ranked first, followed by [^{18}F]FIBT, [^{18}F]flutafuranol (also known as [^{18}F]AZD4694), [^{11}C]BF227, [^{11}C]AZD2184, [^{18}F]flutemetamol, [^{18}F]florbetapir, [^{18}F]FACT, [^{11}C]SB13, [^{18}F]florbetaben, [^{18}F]AV138, and [^{18}F]FDDNP (Table 2). All clinically applied amyloid PET radiotracers had CUI of greater than 3.0 (Table 2).

Fig. 3 shows the simulated SUVR distributions for (A) [^{11}C]PIB, (B) [^{11}C]MeS-IMPY, and (C) [^{18}F]phenylindole-1a in HC, MCI, and AD conditions. [^{11}C]PIB, with the highest CUI of 5.72 (Table 2), showed a small amount of overlapping of SUVR distributions across HC, MCI, and AD conditions. [^{11}C]MeS-IMPY, with a CUI of 1.93 (Table 2), showed greater amount of overlapping and smaller

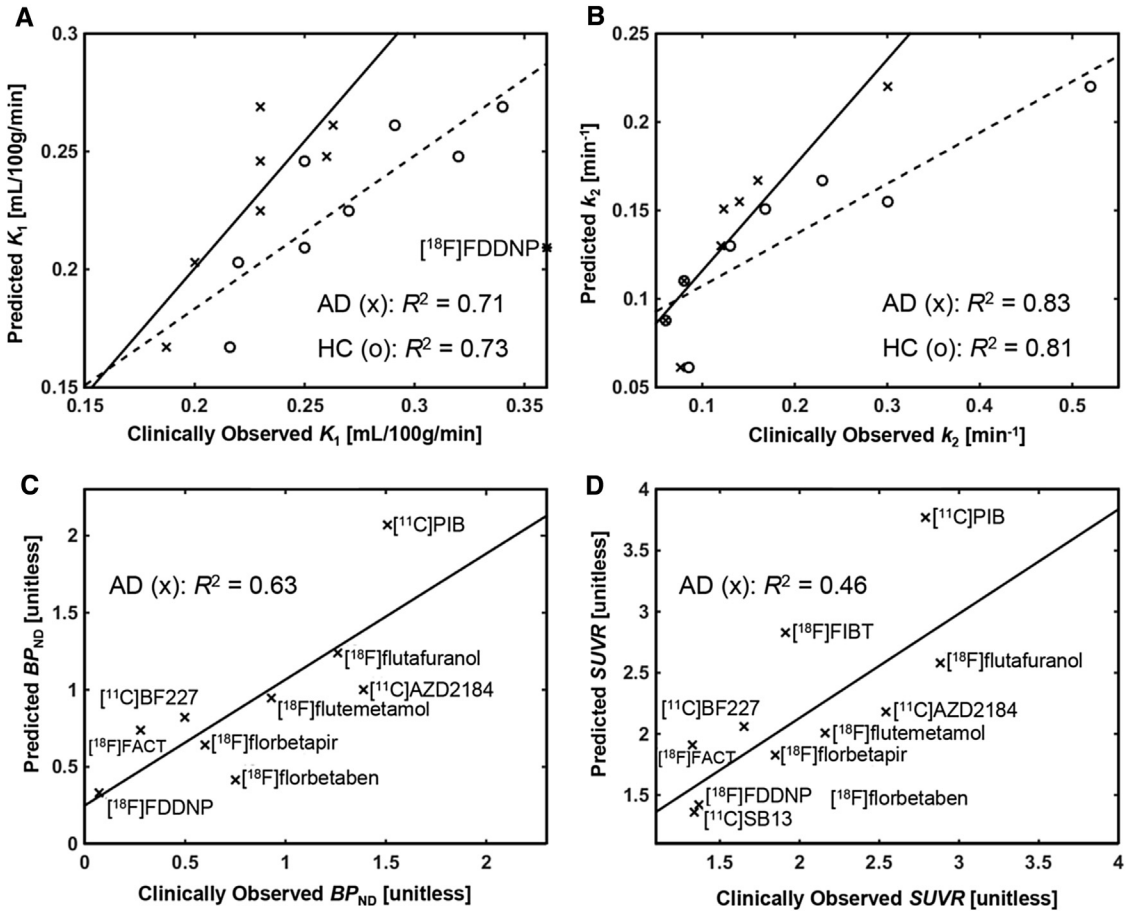

Fig. 2. Correlations of predicted versus clinically observed (A) K_1, (B) k_2, and (C) BP_{ND}, and (D) SUVR. Abbreviations: AD, Alzheimer's disease; HC, healthy control; BP_{ND}, nondisplaceable binding potential; SUVR, standardized uptake value ratio.

differences in the spread of SUVR distributions. The simulated SUVR of [^{11}C]MeS-IMPY was also smaller than that of [^{11}C]PIB. [^{18}F]Phenylindole-1a, with the lowest CUI of 0.10 (Table 2), showed complete overlapping of SUVR distributions across HC, MCI, and AD conditions, and near identical spread of the SUVR distributions in the three conditions. The mean SUVR of [^{18}F]phenylindole-1a was about 1.0 for all three conditions.

The relationships of $\overline{Az}$, $\overline{Es}$, and $\overline{Sr}$ of the 31 amyloid PET radiotracers with the resulting CUI were different (Fig. 4). $\overline{Az}$ and $\overline{Es}$ increased drastically with CUI but plateaued when CUI became greater than 3.0 (Fig. 4A and B). $\overline{Sr}$ increased gradually when CUI was less than 3.0, but increased greatly when CUI became greater than 3.0 (Fig. 4C). $\overline{Az}$ and $\overline{Es}$ showed nonlinear relationship with each other (Fig. 4D). $\overline{Sr}$ was relatively flat when $\overline{Es}$ and $\overline{Az}$ were less than 2.5 and 0.95 but increased steeply after that (Fig. 4E and F).

4. Discussion

In this article, a screening methodology based on the amyloid biomathematical model [8] with CUI was developed to evaluate the clinical usefulness of amyloid PET radiotracers objectively.

4.1. Derivation of CUI

CUI was derived from the product of $\overline{Az}$, $\overline{Es}$, and $\overline{Sr}$ of conditions-pairs of HC-MCI and MCI-AD using equation (10). The relationships of $\overline{Az}$, $\overline{Es}$, and $\overline{Sr}$ with CUI were different (Fig. 4), suggesting that the three evaluation methods assessed different key properties of the radiotracers. This was also observed from the differences in the ranking of the radiotracers based on $\overline{Az}$, $\overline{Es}$, and $\overline{Sr}$ (Table 2). For example, [^{18}F]flutafuranol was ranked the highest based on $\overline{Az}$, whereas [^{11}C]PIB was ranked the highest based on $\overline{Es}$ and [^{11}C]benzofuran-8 was ranked the highest based on $\overline{Sr}$.

The rankings of Az, Es, and Sr were also different between conditions-pairs of HC-MCI and MCI-AD (Table 2). For instance, comparing [^{11}C]PIB and [^{11}C]benzofuran-8, [^{11}C]PIB had higher Az, Es, and Sr for conditions-pair of MCI-AD, whereas [^{11}C]benzofuran-8 had higher Az, Es, and Sr for conditions-pair of HC-MCI (Table 2). This showed that there were differences in diagnostic capability of amyloid PET radiotracers at high and low amyloid loads. Therefore, CUI was derived using conditions-pairs of HC-MCI and MCI-AD. The conditions-pair of HC-AD was excluded because of

Table 2
Az, Es, and Sr of conditions-pairs of HC-MCI and MCI-AD and CUI of 31 amyloid PET radiotracers

	AUROC (Az)		Effect size (Es)		SUVR ratio (Sr)		Averaged			
Radiotracers	HC-MCI	MCI-AD	HC-MCI	MCI-AD	MCI/HC	AD/MCI	Az	Es	Sr	CUI
[^{11}C]PIB	0.979	0.995	2.96	3.64	1.68	1.83	0.987	3.30	1.76	5.72
[^{18}F]FDDNP	0.956	0.989	2.44	3.17	1.12	1.21	0.972	2.80	1.17	3.19
[^{11}C]SB13	0.977	0.992	2.79	3.40	1.11	1.19	0.985	3.10	1.15	3.50
[^{18}F]florbetaben	0.968	0.987	2.57	3.13	1.14	1.23	0.977	2.85	1.19	3.30
[^{11}C]BF227	0.981	0.992	2.95	3.46	1.30	1.46	0.987	3.20	1.38	4.35
[^{18}F]AV138	0.964	0.983	2.63	2.95	1.15	1.23	0.974	2.79	1.19	3.22
[^{18}F]flutemetamol	0.977	0.989	2.87	3.28	1.29	1.44	0.983	3.08	1.37	4.13
[^{18}F]florbetapir	0.977	0.993	2.78	3.44	1.23	1.38	0.985	3.11	1.31	4.01
[^{11}C]AZD2184	0.978	0.991	2.94	3.26	1.33	1.50	0.984	3.10	1.41	4.32
[^{18}F]flutafuranol	0.985	0.993	2.94	3.39	1.42	1.61	0.989	3.16	1.52	4.74
[^{18}F]FACT	0.973	0.992	2.66	3.40	1.25	1.42	0.983	3.03	1.34	3.97
[^{18}F]FIBT	0.981	0.991	2.97	3.37	1.49	1.62	0.986	3.17	1.56	4.87
[^{11}C]6-Me-BTA-1	0.774	0.885	1.03	1.74	1.01	1.03	0.830	1.38	1.02	1.17
[^{11}C]BTA-1	0.945	0.981	2.20	3.07	1.04	1.07	0.963	2.64	1.06	2.68
[^{18}F]FMAPO	0.840	0.927	1.39	2.07	1.03	1.06	0.884	1.73	1.04	1.59
[^{18}F]FPEG-stilbenes-12a*	0.910	0.958	1.85	2.50	1.05	1.10	0.934	2.18	1.07	2.18
[^{11}C]Benzofuran-8*	0.978	0.991	2.91	3.21	1.89	1.78	0.984	3.06	1.83	5.52
[^{18}F]FPEGN3-styrylpyridine-2*	0.808	0.907	1.30	1.85	1.03	1.05	0.857	1.57	1.04	1.40
[^{11}C]MeS-IMPY	0.866	0.963	1.62	2.45	1.02	1.05	0.915	2.03	1.04	1.93
[^{18}F]Indole-14*	0.977	0.984	2.89	3.00	1.27	1.35	0.981	2.95	1.31	3.77
[^{18}F]Indoline-8*	0.958	0.985	2.45	3.03	1.11	1.19	0.971	2.74	1.15	3.06
[^{11}C]Benzothiazole-6a*	0.943	0.984	2.29	3.05	1.05	1.10	0.963	2.67	1.08	2.77
[^{11}C]Benzothiazole-6b*	0.967	0.988	2.67	3.23	1.09	1.16	0.978	2.95	1.12	3.24
[^{11}C]Benzothiazole-6c*	0.970	0.991	2.74	3.33	1.09	1.17	0.980	3.03	1.13	3.36
[^{18}F]Benzothiazole-2*	0.635	0.768	0.498	0.988	1.01	1.02	0.701	0.743	1.02	0.530
[^{18}F]Benzothiazole-5*	0.631	0.737	0.450	0.865	1.01	1.02	0.684	0.658	1.01	0.456
[^{18}F]MK3328	0.913	0.974	1.99	2.78	1.07	1.12	0.944	2.39	1.10	2.47
[^{18}F]FIAR	0.683	0.803	0.682	1.22	1.01	1.03	0.743	0.953	1.02	0.723
[^{18}F]Benzoxazole-24*	0.960	0.988	2.54	3.22	1.12	1.20	0.974	2.88	1.16	3.25
[^{18}F]Pyridinylbenzoxazole-32*	0.966	0.987	2.53	3.16	1.13	1.22	0.977	2.84	1.18	3.26
[^{18}F]Phenylindole-1a*	0.554	0.548	0.168	0.200	1.00	1.00	0.551	0.184	1.00	0.102

Abbreviations: AD, Alzheimer's disease; AUROC, area under the receiver operating characteristic curve; CUI, clinical usefulness index; HC, healthy control; MCI, mild cognitive impaired; PET, positron emission tomography; SUVR, standardized uptake value ratio.

NOTE. The radiotracers listed from [^{11}C]PIB to [^{18}F]FIBT are clinically applied radiotracers and the rest are candidate radiotracers. Az, Es, Sr, and CUI are unitless.

*Simplified name with compound number or alphabet, as reported in the literature, used when generic name or institute code name (supplied by the author) was not available.

replication of results, and if used individually, it would not be able to differentiate the performance of the radiotracers at low and high amyloid loads.

The range of individual Az, Es, and Sr was smaller than CUI (Table 2). Az had a small range of values from 0.548 to 0.995 (Table 2), which resulted in many radiotracers having the same values of $\overline{Az}$. Although the range of values of E*s* of 0.168 to 3.64 was reasonably broad (Table 2), it only considered the strength of the differences between the measured outcomes of two conditions with variations. Likewise, Sr, which ranged from 1.00 to 1.89, only showed the magnitude of the differences in mean SUVR between two conditions (Table 2).

The combination of Az, Es, and Sr integrated their strengths, including statistical significance (mainly Es), sample variability (mainly Az and Es), and measurement precision (mainly Az and Sr). Greater spread in $\overline{Az}$ and $\overline{Es}$ was observed when CUI was smaller than 3.0, whereas greater spread in $\overline{Sr}$ was observed when CUI was greater than 3.0. The combination of Az, Es, and Sr thus complemented each other and resulted in a broader range of CUI of 0.10 to 5.72 (Table 2). This allowed for clear differentiation of the clinical usefulness of the amyloid PET radiotracers.

4.2. Validation of CUI

The SUVR distributions simulated across the three subject conditions will affect the CUI of the amyloid PET radiotracers. Variations in B_{avail} by 80%, 35%, and 20% in HC, MCI, and AD conditions, respectively, were chosen to reflect the variations in amyloid load under HC, MCI, and AD conditions [40], and to simulate SUVR distributions similar to that observed clinically [2,3]. The position of the median, box length, and whisker length of simulated boxplot were evenly distributed due to the use of 1000 SUVRs, which differed from clinical data as the sample size reported was generally smaller. However, the overall spread of

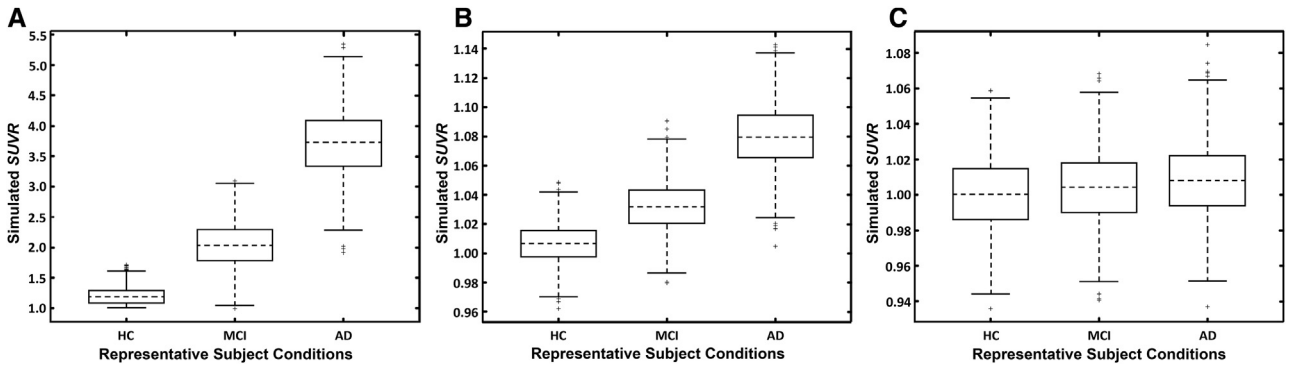

Fig. 3. Simulated SUVR distributions across HC, MCI, and AD conditions for three amyloid PET radiotracers. (A) [^{11}C]PIB; (B) [^{11}C]MeS-IMPY; and (C) [^{18}F]phenylindole-1a. Abbreviations: AD, Alzheimer's disease; HC, healthy control; MCI, mild cognitive impaired; PET, positron emission tomography; SUVR, standardized uptake value ratio.

simulated SUVR distributions of [^{11}C]PIB was close to that observed clinically (Fig. 3A) [2,4], thus showing that the variations in B_{avail} were suitable. Poor radiotracers such as [^{18}F]phenylindole-1a and [^{18}F]FMAPO displayed huge overlapping of SUVR distributions across all subject conditions as observed in Fig. 3B and C.

Different scaling factors were applied in equations (3), (5), and (6) in the current model compared with previously developed model [7,8] to scale the differences between predicted and clinically observed data. The scaling factor for K_1 in Guo's central nervous system model was 3.43 [7], whereas a scaling factor of 1.23 was applied in the current model. The difference was probably because of the type of in vivo data used. Guo et al. used in vivo data measured from pig [7], whereas in vivo data measured from human were used for our evaluation. In Guo's model, apparent aqueous volumes in plasma and tissue ($V_{aq\_P}/V_{aq\_T} = 1.09$) were used to derive k_2 [7]. A scaling factor of 1.15 was used in our model. The difference was small and might be because of slight differences between HC and AD conditions. The correlations between predicted and clinically observed K_1, k_2, BP_{ND}, and SUVR were relatively similar to previously evaluated results [8] (Fig. 2). This indicated that the results can be replicated using SUVR.

4.3. Limitations of CUI

The model under CUI does not consider nonspecific binding in white matter. In amyloid PET imaging, white matter retention may lead to inaccuracies in cortical SUVR measurements [3,22]. However, some studies have shown that the amount of white matter retention was independent of the amount of amyloid load present in the subjects as supported by the lack of differences in white matter

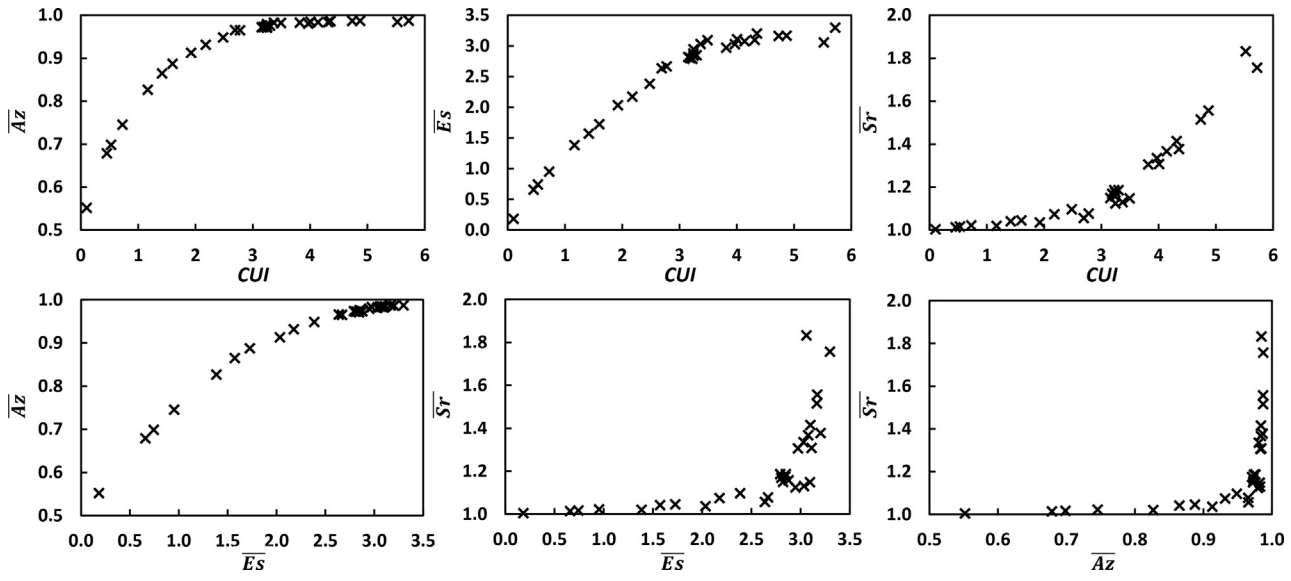

Fig. 4. Relationships among $\overline{Az}$, $\overline{Es}$, $\overline{Sr}$, and CUI of 31 amyloid PET radiotracers. Abbreviations: CUI, clinical usefulness index; PET, positron emission tomography.

retention between HC and AD [4,22,46,47]. Studies have also reported that white matter retention did not limit the quantification of cortical uptake of some amyloid PET radiotracer [4,5,22,48]. The SUVR measurements in the white matter do not correlate with cortical SUVR measurements, and white matter modifications may be because of normal aging or other diseases. As such, the screening methodology with CUI was developed to judge the clinical usefulness of a radiotracer based on its cortical amyloid binding capability.

The current list of CUI was determined using K_D or K_i obtained from the literature (Table 1). K_D is the only in vitro input, whereas the others were in silico parameters (Fig 1A). For consistent outcome comparison, K_D was selected over K_i, as reported K_i differed depending on the competitor. K_i was selected if it was measured with itself or IMPY as a competitor. IMPY was chosen because of the availability of a large number of K_i measured with IMPY as a competitor, which allowed for the comparison of many radiotracers. Reliable comparison of radiotracers can be achieved by using K_D measured using the same experimental protocol within an institution. The use of CUI enables cross-institution comparison with the use of a reference or clinically applied radiotracer (e.g., [^{11}C]PIB).

Amyloid PET radiotracers such as [^{11}C]PIB, [^{11}C]BF227, and [^{18}F]FDDNP had been reported to bind to neurofibrillary tangles [48]. As [^{18}F]FDDNP had a lower binding affinity for amyloid fibrils, it showed lower cortical uptake in AD [15]. The current amyloid biomathematical model did not include the effect of tau binding because the target was amyloid protein [8]. Despite the use of only K_D of Aβ fibrils, the CUI rankings of clinically applied amyloid PET radiotracers (Table 2) reflected close to reported clinical results. Therefore, the model showed applicability in evaluating the clinical usefulness of amyloid PET radiotracers. For proper application of the screening methodology and comparable CUI, in vitro binding studies to both Aβ fibrils and tau protein and comparison of CUI with one clinically applied amyloid PET radiotracer (e.g., [^{11}C]PIB) are recommended.

4.4. Applications of CUI

To determine the feasibility of CUI, we compared CUI with data of clinically applied radiotracers from the literature. *[^{18}F]flutafuranol* versus *[^{11}C]AZD2184*: [^{11}C]AZD2184 (distribution volume ratio, 1.7) showed relatively similar cortical binding to [^{18}F]flutafuranol (distribution volume ratio, 1.6) in AD subjects [49]. In our simulations, [^{18}F]flutafuranol (CUI = 4.74, ranked fourth) and [^{11}C]AZD2184 (CUI = 4.32, ranked sixth) showed relatively similar clinical usefulness. *[^{11}C]BF227* versus *[^{18}F]FACT*: [^{11}C]BF227 showed greater significant differences in cortical SUVR between HC and AD subjects than [^{18}F]FACT [41], which allowed for clearer differentiation of subject groups. [^{11}C]BF227 (CUI = 4.35, ranked fifth) had higher CUI than [^{18}F]FACT (CUI = 3.97, ranked ninth) in our simulations. [^{18}F]florbetapir versus [^{18}F]AV138: [^{18}F]florbetapir and [^{18}F]AV138 showed similar SUVR in precuneus, but [^{18}F]florbetapir was reported to have better pharmacokinetics and pharmacodynamics compared with [^{18}F]AV138 in clinical trial [50]. [^{18}F]florbetapir (CUI = 4.01, ranked eighth) also had higher CUI than [^{18}F]AV138 (CUI = 3.22, ranked 17th) in our simulations. *[^{11}C]PIB* versus *[^{18}F]flutemetamol* versus *[^{18}F]florbetapir*: In terms of clinical cortical uptakes in MCI and AD subjects, [^{11}C]PIB was the highest, followed by [^{18}F]flutemetamol then [^{18}F]florbetapir, without partial volume correction [3]. Likewise, our simulation results showed that [^{11}C]PIB had the highest CUI of 5.72, followed by [^{18}F]flutemetamol (CUI = 4.13, ranked seventh) then [^{18}F]florbetapir (CUI = 4.01, ranked eighth). The ranking of CUI was close to clinical results, thus showing that the screening methodology with CUI attests to its potential in evaluating the clinical usefulness of amyloid candidate radiotracers.

All clinically applied radiotracers had CUI of greater than 3.0 (Table 2). Thus, a minimum CUI of 3.0 is recommended to move candidate radiotracers for further evaluation. We recommend comparing candidate radiotracers with a clinically applied radiotracer (e.g., [^{11}C]PIB) to evaluate their possible clinical performance with respect to the clinical performance of clinically applied radiotracers. The screening methodology can also be used to predict other parameters of interest, such as BP_{ND}, which can be applied as the outcome parameter of interest in CUI. We believed that the screening methodology with CUI can be extended to other similar types of radiotracers (e.g., tau radiotracers). However, the binding affinities to both Aβ fibrils and tau protein must be measured to ensure that the tau radiotracer has higher selectivity to tau protein than Aβ fibrils. We are currently evaluating the use of the screening methodology for tau radiotracers. Despite the greater challenges faced in tau imaging compared with amyloid imaging (e.g., off-target binding), we believe the results from the screening methodology can shed some insights into the binding behavior of tau radiotracers. On the whole, the screening methodology with CUI, allows for simultaneous and objective comparison of candidate radiotracers during radiotracer development.

Acknowledgments

The authors would like to thank Dr Qi Guo of AbbVie Inc (US) for her feedback and advice on this project.
Funding: This study was supported by Grants-in-Aid for Scientific Research (B) (No. 17H04118) and (C) (No. 15K08687) from the Ministry of Education, Culture, Sports, Science and Technology (MEXT), Japanese Government.

RESEARCH IN CONTEXT

1. Systematic review: The authors proposed a screening methodology using a biomathematical model and clinical usefulness index (*CUI*) to facilitate the development of amyloid radiotracers. 31 (12 clinically-applied, 19 candidates) amyloid PET radiotracers were gathered from the literature. The predicted 1-tissue compartment kinetic parameters and standardized uptake values ratio (*SUVR*) were compared with the available clinically-observed values. The outcome *CUI* were compared to their reported clinical comparison results.
2. Interpretation: The *CUI* ranking of clinically-applied radiotracers were close to their reported clinical results, thus attesting to the applicability of the screening methodology for screening amyloid radiotracers. Future directions: The manuscript forms the backbone for developing a screening methodology to support the development of not only amyloid but tau radiotracers.
3. Future directions: (1) evaluating the feasibility of extending the screening methodology to screen tau radiotracers, (2) if not, determining the underlying issues to develop an improved screening methodology for tau radiotracers.

References

[1] Perrin RJ, Fagan AM, Holtzman DM. Multimodal techniques for diagnosis and prognosis of Alzheimer's disease. Nature 2009; 461:916–22.

[2] Hatashita S, Yamasaki H, Suzuki Y, Tanaka K, Wakebe D, Hayakawa H. [18F]Flutemetamol amyloid-beta PET imaging compared with [11C]PIB across the spectrum of Alzheimer's disease. Eur J Nucl Med Mol Imaging 2014;41:290–300.

[3] Landau SM, Thomas BA, Thurfjell L, Schmidt M, Margolin R, Mintun M, et al. Amyloid PET imaging in Alzheimer's disease: a comparison of three radiotracers. Eur J Nucl Med Mol Imaging 2014;41:1398–407.

[4] Vandenberghe R, Van Laere K, Ivanoiu A, Salmon E, Bastin C, Triau E, et al. 18F-flutemetamol amyloid imaging in Alzheimer disease and mild cognitive impairment: a phase 2 trial. Ann Neurol 2010;68:319–29.

[5] Barthel H, Gertz HJ, Dresel S, Peters O, Bartenstein P, Buerger K, et al. Cerebral amyloid-β PET with florbetaben (18 F) in patients with Alzheimer's disease and healthy controls: a multicentre phase 2 diagnostic study. Lancet Neurol 2011;10:424–35.

[6] Agdeppa ED, Spilker ME. A review of imaging agent development. AAPS J 2009;11:286–99.

[7] Guo Q, Brady M, Gunn RN. A biomathematical modeling approach to central nervous system radioligand discovery and development. J Nucl Med 2009;50:1715–23.

[8] Arakawa Y, Nai Y, Shidahara M, Furumoto S, Seki C, Okamura N, et al. Prediction of the clinical standardized uptake value ratio in amyloid PET imaging using a biomathematical modeling approach towards the efficient development of a radioligand. J Nucl Med 2017; 58:1285–92.

[9] Fawcett T. An introduction to ROC analysis. Pattern Recogn Lett 2006;27:861–74.

[10] Okamura N, Furumoto S, Fodero-Tavoletti MT, Mulligan RS, Harada R, Yates P, et al. Non-invasive assessment of Alzheimer's disease neurofibrillary pathology using 18F-THK5105 PET. Brain 2014; 137:1762–71.

[11] Mathis CA, Wang Y, Holt DP, Huang GF, Debnath ML, Klunk WE. Synthesis and evaluation of 11 C-labeled 6-substituted 2-arylbenzothiazoles as amyloid imaging agents. J Med Chem 2003; 46:2740–54.

[12] Klunk WE. Binding of the positron emission tomography tracer Pittsburgh Compound-B reflects the amount of amyloid in Alzheimer's disease brain but not in transgenic mouse brain. J Neurosci 2005; 25:10598–606.

[13] Ikonomovic MD, Klunk WE, Abrahamson EE, Mathis CA, Price JC, Tsopelas ND, et al. Post-mortem correlates of in vivo PiB-PET amyloid imaging in a typical case of Alzheimer's disease. Brain 2008; 131:1630–45.

[14] Johnson AE, Jeppsson F, Sandell J, Wensbo D, Neelissen JA, Juréus A, et al. AZD2184: a radioligand for sensitive detection of β-amyloid deposits. J Neurochem 2009;108:1177–86.

[15] Thompson PW, Ye L, Morgenstern JL, Sue L, Beach TG, Judd DJ, et al. Interaction of the amyloid imaging tracer FDDNP with hallmark Alzheimer's disease pathologies. J Neurochem 2009;109:623–30.

[16] Agdeppa ED, Kepe V, Liu J, Flores-Torres S, Satyamurthy N, Petric A, et al. Binding characteristics of radiofluorinated 6-dialkylamino-2-naphthylethylidene derivatives as positron emission tomography imaging probes for beta-amyloid plaques in Alzheimer's disease. J Neurosci 2001;21:RC189.

[17] Kung MP, Hou C, Zhuang ZP, Skovronsky D, Kung HF. Binding of two potential imaging agents targeting amyloid plaques in postmortem brain tissues of patients with Alzheimer's disease. Brain Res 2004; 1025:98–105.

[18] Choi SR, Golding G, Zhuang Z, Zhang W, Lim N, Hefti F, et al. Preclinical properties of 18F-AV-45: a PET agent for Abeta plaques in the brain. J Nucl Med 2009;50:1887–94.

[19] Furumoto S, Okamura N, Iwata R, Yanai K, Arai H, Kudo Y. Recent advances in the development of amyloid imaging agents. Curr Top Med Chem 2007;7:1773–89.

[20] Chandra R, Oya S, Kung MP, Hou C, Jin LW, Kung HF. New diphenylacetylenes as probes for positron emission tomographic imaging of amyloid plaques. J Med Chem 2007;50:2415–23.

[21] Juréus A, Swahn BM, Sandell J, Jeppsson F, Johnson AE, Johnström P, et al. Characterization of AZD4694, a novel fluorinated Aβ plaque neuroimaging PET radioligand: AZD4694 a new amyloid PET radioligand. J Neurochem 2010;114:784–94.

[22] Villemagne VL, Klunk WE, Mathis CA, Rowe CC, Brooks DJ, Hyman BT, et al. Aβ imaging: feasible, pertinent, and vital to progress in Alzheimer's disease. Eur J Nucl Med Mol Imaging 2012; 39:209–19.

[23] Yousefi BH, von Reutern B, Scherübl D, Manook A, Schwaiger M, Grimmer T, et al. FIBT versus florbetaben and PiB: a preclinical comparison study with amyloid-PET in transgenic mice. EJNMMI Res 2015;5:20.

[24] Klunk WE, Wang Y, Huang GF, Debnath ML, Holt DP, Mathis CA. Uncharged thioflavin-T derivatives bind to amyloid-beta protein with high affinity and readily enter the brain. Life Sci 2001; 69:1471–84.

[25] Mathis CA, Bacskai BJ, Kajdasz ST, McLellan ME, Frosch MP, Hyman BT, et al. A lipophilic thioflavin-T derivative for positron emission tomography (PET) imaging of amyloid in brain. Bioorg Med Chem Lett 2002;12:295–8.

[26] Zhang W, Oya S, Kung MP, Hou C, Maier DL, Kung HF. F-18 stilbenes as PET imaging agents for detecting beta-amyloid plaques in the brain. J Med Chem 2005;48:5980–8.

[27] Zhang W, Oya S, Kung MP, Hou C, Maier DL, Kung HF. F-18 polyethyleneglycol stilbenes as PET imaging agents targeting Aβ aggregates in the brain. Nucl Med Biol 2005;32:799–809.
[28] Ono M, Kawashima H, Nonaka A, Kawai T, Haratake M, Mori H, et al. Novel benzofuran derivatives for PET imaging of β-amyloid plaques in Alzheimer's disease brains. J Med Chem 2006;49:2725–30.
[29] Zhang W, Kung MP, Oya S, Hou C, Kung HF. 18F-labeled styrylpyridines as PET agents for amyloid plaque imaging. Nucl Med Biol 2007;34:89–97.
[30] Seneca N, Cai L, Liow JS, Zoghbi SS, Gladding RL, Hong J, et al. Brain and whole-body imaging in nonhuman primates with [11C] MeS-IMPY, a candidate radioligand for β-amyloid plaques. Nucl Med Biol 2007;34:681–9.
[31] Qu W, Choi SR, Hou C, Zhuang Z, Oya S, Zhang W, et al. Synthesis and evaluation of indolinyl- and indolylphenylacetylenes as PET imaging agents for β-amyloid plaques. Bioorg Med Chem Lett 2008; 18:4823–7.
[32] Serdons K, Verduyckt T, Vanderghinste D, Borghgraef P, Cleynhens J, Van Leuven F, et al. 11C-labelled PIB analogues as potential tracer agents for in vivo imaging of amyloid β in Alzheimer's disease. Eur J Med Chem 2009;44:1415–26.
[33] Serdons K, Verduyckt T, Vanderghinste D, Cleynhens J, Borghgraef P, Vermaelen P, et al. Synthesis of 18F-labelled 2-(4′-fluorophenyl)-1,3-benzothiazole and evaluation as amyloid imaging agent in comparison with [11C]PIB. Bioorg Med Chem Lett 2009;19:602–5.
[34] Serdons K, Terwinghe C, Vermaelen P, Van Laere K, Kung H, Mortelmans L, et al. Synthesis and evaluation of 18 F-labeled 2-phenylbenzothiazoles as positron emission tomography imaging agents for amyloid plaques in Alzheimer's disease. Eur J Med Chem 2009;52:1428–37.
[35] Harrison ST, Mulhearn J, Wolkenberg SE, Miller PJ, O'Malley SS, Zeng Z, et al. Synthesis and evaluation of 5-fluoro-2-aryloxazolo [5,4-b]pyridines as β-amyloid PET ligands and identification of MK-3328. ACS Med Chem Lett 2011;2:498–502.
[36] Watanabe H, Ono M, Kimura H, Kagawa S, Nishii R, Fuchigami T, et al. A dual fluorinated and iodinated radiotracer for PET and SPECT imaging of β-amyloid plaques in the brain. Bioorg Med Chem Lett 2011;21:6519–22.
[37] Cui M, Ono M, Kimura H, Ueda M, Nakamoto Y, Togashi K, et al. Novel 18 F-labeled benzoxazole derivatives as potential positron emission tomography probes for imaging of cerebral β-amyloid plaques in Alzheimer's disease. J Med Chem 2012;55:9136–45.
[38] Cui M, Wang X, Yu P, Zhang J, Li Z, Zhang X, et al. Synthesis and evaluation of novel 18 F labeled 2-pyridinylbenzoxazole and 2-pyridinylbenzothiazole derivatives as ligands for positron emission tomography (PET) imaging of β-amyloid plaques. J Med Chem 2012; 55:9283–96.
[39] Fu H, Yu L, Cui M, Zhang J, Zhang X, Li Z, et al. Synthesis and biological evaluation of 18F-labled 2-phenylindole derivatives as PET imaging probes for β-amyloid plaques. Bioorg Med Chem 2013; 21:3708–14.
[40] Svedberg MM, Hall H, Hellström-Lindahl E, Estrada S, Guan Z, Nordberg A, et al. [11C]PIB-amyloid binding and levels of Aβ40 and Aβ42 in postmortem brain tissue from Alzheimer patients. Neurochem Int 2009;54:347–57.
[41] Shidahara M, Watabe H, Tashiro M, Okamura N, Furumoto S, Watanuki S, et al. Quantitative kinetic analysis of PET amyloid imaging agents [11C]BF227 and [18F]FACT in human brain. Nucl Med Biol 2015;42:734–44.
[42] Yousefi BH, Manook A, Grimmer T, Arzberger T, von Reutern B, Henriksen G, et al. Characterization and first human investigation of FIBT, a novel fluorinated Aβ plaque neuroimaging PET radioligand. ACS Chem Neurosci 2015;6:428–37.
[43] Guo Q, Owen DR, Rabiner EA, Turkheimer FE, Gunn RN. Identifying improved TSPO PET imaging probes through biomathematics: the impact of multiple TSPO binding sites in vivo. Neuroimage 2012; 60:902–10.
[44] Logan J, Fowler JS, Volkow ND, Ding YS, Wang GJ, Alexoff DL. A strategy for removing the bias in the graphical analysis method. J Cereb Blood Flow Metab 2001;21:307–20.
[45] Ikoma Y, Ito H, Arakawa R, Okumura M, Seki C, Shidahara M, et al. Error analysis for PET measurement of dopamine D2 receptor occupancy by antipsychotics with [11C]raclopride and [11C]FLB 457. Neuroimage 2008;42:1285–94.
[46] Furumoto S, Okamura N, Furukawa K, Tashiro M, Ishikawa Y, Sugi K, et al. A 18F-labeled BF-227 derivative as a potential radioligand for imaging dense amyloid plaques by positron emission tomography. Mol Imaging Biol 2013;15:497–506.
[47] Cselenyi Z, Jonhagen ME, Forsberg A, Halldin C, Julin P, Schou M, et al. Clinical validation of 18F-AZD4694, an amyloid-specific PET radioligand. J Nucl Med 2012;53:415–24.
[48] Harada R, Okamura N, Furumoto S, Tago T, Maruyama M, Higuchi M, et al. Comparison of the binding characteristics of [18F]THK-523 and other amyloid imaging tracers to Alzheimer's disease pathology. Eur J Nucl Med Mol Imaging 2013;40:125–32.
[49] Forsberg A, Mattsson P, Cselényi Z, Jönhagen ME, Juréus A, Jeppsson F. Sensitive and specific amyloid-b PET imaging using the three novel radioligands [18F]AZD4694, [11C]AZD2184 and [11C] AZD2995 in Alzheimer's disease patients. J Cereb Blood Flow Metab 2012;32:S100–27.
[50] Carpenter AP, Pontecorvo MJ, Hefti FF, Skovronsky DM. The use of the exploratory IND in the evaluation and development of 18F-PET radiopharmaceuticals for amyloid imaging in the brain: a review of one company's experience. Q J Nucl Med Mol Imaging 2009;53:387–93.